REPORT DOCUMENTATION PAGE

Form Approved
OMB No. 0704-0188

1. REPORT DATE *(DD-MM-YYYY)*	**2. REPORT TYPE**	**3. DATES COVERED** *(From - To)*
26-03-2007	Technical Paper and Briefing Charts	

4. TITLE AND SUBTITLE

Experimental and Numerical Investigations of RP-2 Under High Heat Fluxes

5a. CONTRACT NUMBER

5b. GRANT NUMBER

5c. PROGRAM ELEMENT NUMBER

6. AUTHOR(S)
M.C. Billingsley, H.Y. Lyu, R.W. Bates

5d. PROJECT NUMBER
48470244

5e. TASK NUMBER

5f. WORK UNIT NUMBER

7. PERFORMING ORGANIZATION NAME(S) AND ADDRESS(ES)

AFRL/PRSA
10 E. Saturn Blvd.
Edwards AFB CA 93524-7680

8. PERFORMING ORGANIZATION REPORT NUMBER

AFRL-PR-ED-TP-2007-150

9. SPONSORING / MONITORING AGENCY NAME(S) AND ADDRESS(ES)

Air Force Research Laboratory (AFMC)
AFRL/PRS
5 Pollux Drive
Edwards AFB CA 93524-7048

10. SPONSOR/MONITOR'S ACRONYM(S)

11. SPONSOR/MONITOR'S NUMBER(S)
AFRL-PR-ED-TP-2007-150

12. DISTRIBUTION / AVAILABILITY STATEMENT

Distribution A: Approved for public release; distribution unlimited. (Public Affairs No. 07125A).

13. SUPPLEMENTARY NOTES
Presented at the JANNAF 54th Propulsion Meeting/3rd Liquid Propulsion Subcommittee/2nd Spacecraft Propulsion Subcommittee/5th Modeling and Simulation Subcommittee Joint Meeting, Denver, CO, 14-17 May 2007.

14. ABSTRACT

Interest in developing reusable, long-life, liquid hydrocarbon fueled rocket engines has continued to grow in recent years. Of critical importance in designing and developing an engine with these characteristics is of course the fuel and its impact on potential cooling schemes. For several years now, the Air Force Research Laboratory Propulsion Directorate has been developing the capability to examine the thermal performance of newly emerging petroleum distillate fuels such as RP-2, an advanced grade of ultra-low sulfur rocket kerosene. This paper reports recent experiments and numerical simulations of RP-2 cooled thermal stability tests conducted in the AFRL High Heat Flux Facility located at Edwards AFB, CA. Heat transfer measurements and simulations of those experiments using Metacomp's CFD++ conjugate heat transfer capability were conducted over heat fluxes ranging from 2-10 BTU/in2/s, channel velocities from 26-165 ft/s, and wall temperatures from 840-1135°F. A Nusselt number correlation comparison of experimental results to well-known Dittus-Boelter and Sieder-Tate correlations and the NASA/GRC correlation of Stiegemeier et. al is presented for Reynolds numbers between 5,000-35,000. Computational comparisons with experimental measurements are made and represent the first steps in producing a validated predictive computational capability.

15. SUBJECT TERMS

16. SECURITY CLASSIFICATION OF:			**17. LIMITATION OF ABSTRACT**	**18. NUMBER OF PAGES**	**19a. NAME OF RESPONSIBLE PERSON**
					Dr. Ronald Bates
a. REPORT	**b. ABSTRACT**	**c. THIS PAGE**	SAR	32	**19b. TELEPHONE NUMBER** *(include area code)*
Unclassified	**Unclassified**	**Unclassified**			(661) 275-5664

Experimental and Numerical Investigations of RP-2 Under High Heat Fluxes

M. C. Billingsley, H. Y. Lyu, R. W. Bates
Air Force Research Laboratory, Propulsion Directorate
Edwards AFB, CA 93524

54th Joint Army-Navy-NASA-Air Force (JANNAF) Propulsion Meeting (JPM) / 5th Modeling & Simulation Subcommittee (MSS) / 3rd Liquid Propulsion Subcommittee (LPS) / 2nd Spacecraft Propulsion Subcommittee (SPS) Joint Meeting
Denver, CO, 14-17 May 2007

ABSTRACT

Interest in developing reusable, long-life, liquid hydrocarbon fueled rocket engines has continued to grow in recent years. Of critical importance in designing and developing an engine with these characteristics is of course the fuel and its impact on potential cooling schemes. For several years now, the Air Force Research Laboratory Propulsion Directorate has been developing the capability to examine the thermal performance of newly emerging petroleum distillate fuels such as RP-2, an advanced grade of ultra-low sulfur rocket kerosene. This paper reports recent experiments and numerical simulations of RP-2 cooled thermal stability tests conducted in the AFRL High Heat Flux Facility located at Edwards AFB, CA. Heat transfer measurements and simulations of those experiments using Metacomp's CFD++ conjugate heat transfer capability were conducted over heat fluxes ranging from 2-10 BTU/in^2/s, channel velocities from 26-165 ft/s, and wall temperatures from 840-1135°F. A Nusselt number correlation comparison of experimental results to well-known Dittus-Boelter and Sieder-Tate correlations and the NASA/GRC correlation of Stiegemeier et. al is presented for Reynolds numbers between 5,000-35,000. Computational comparisons with experimental measurements are made and represent the first steps in producing a validated predictive computational capability.

INTRODUCTION

RP-2 as described in MIL-DTL-25576E is an advanced grade of rocket kerosene with less than 100 ppb total sulfur content, making it an ideal candidate for use in liquid fueled hydrocarbon rocket engines where long-life and reusability are important. The role of sulfur in thermal decomposition of rocket kerosene and corrosion of copper rocket chamber materials has been previously reported by research groups at UTRC, Aerojet, NASA, and AFRL. Several recent investigations have reported the promising reduction in deposit formation and increased wall-temperature cooling capability of RP-2. This work reports initial investigations of heat transfer performance in the AFRL High Heat Flux Facility (HHFF), using RP-2 as a coolant. Coking limits and morphology of deposition, and the roles of sulfur concentration, type, dissolved oxygen concentration, and wetted surface features will be reported in future work.

Comparisons of numerically predicted heat transfer are presented in this paper using conjugate heat transfer calculations of the experiments conducted. Metacomp's CFD++ code was used primarily to establish a baseline for future comparisons where wall temperatures will be increased and coking deposition is expected to occur. Although AFRL has been working to establish a good physical model for thermal decomposition processes and chemistry, implementation of that model is still under development and validation with Metacomp Technologies through an SBIR. Future work will report progress in prediction and modeling of both deposition and heat transfer processes. For this work, experimental conditions not expected to be affected by deposition were chosen to facilitate comparison of heat transfer predictions with measured results. Ultimately, this work represents the first steps in the process of validation

experiments necessary to produce improved analysis and predictive capability for computational tools, anchored by experiments in the HHFF, for advanced rocket chamber design.

CFD++ is a commercially available computational fluid dynamics software package designed by Metacomp Technologies, Inc. CFD++ is capable of handling the multi-physics phenomena encountered in a general fluid problem. In addition, CFD++ provides advanced turbulence models and wall treatments, including a "solve-to-wall" option, and all these features are required to capture the relevant phenomena present in the current research. The goal of this research is to build a comprehensive conjugate heat transfer simulation, in hope that such a model can be used as a design and experimental data analysis tool. However, the authors took an incremental approach to building the computational model: starting with a simple pipe flow model; proceeding to a conjugate pipe flow calculation; and evolving into a system model including all peripheries related to the fluid channel. The whole system model thus includes heater block, fluid channel, and tube holder block. With this incremental approach, one can examine and compare the experimental and computational results in great detail, identifying critical components to bridge the discrepancies, and exploring future research needs. The incremental approach also favors the computational efforts, as one expects a greater computational resource to be required as the model becomes more sophisticated.

In the simple pipe flow model, wall temperature is specified as a boundary condition. The emphasis in this phase is to examine basic flow structures, to evaluate computational tool's capability, to consider RP-2 property effects, and to identify wall treatment and grid issues. As the model evolves into a conjugate heat transfer calculation, one would expect the interaction between propellant and heat conducting devices to become more active. One would also expect that competing heat paths would affect the propellant heat transfer characteristics, and eventually a transient consideration may be required for rate sensitive processes. In this paper, the authors report the progress of this incremental approach, and present some findings in this pursuit.

EXPERIMENTAL AND COMPUTATIONAL SETUP

EXPERIMENTAL CONFIGURATION

A large copper heater block provided asymmetric heat transfer to the fuel passing through the test section. This copper thermal mass was conductively heated by 25 cartridge heaters. Two heater types were employed: split-sheath heaters controlled through software with manual power input; and custom-made heaters with proportional-integral-derivative (PID) control of internal heater temperature. These heaters maintained block temperatures between 900-1400°F (measured near the base of the heater block). Electrical consumption by the cartridge heaters was on the order of 5 kW.

The High Heat Flux Facility (HHFF) was designed with the flexibility of accommodating a variety of test section sizes and shapes. The results presented in this paper were obtained using 0.125-in. (OD) round copper tubing with 0.032-in. wall thickness. Initially, the tube was sandwiched between two holder blocks, as seen in part a) of Figure 1. The large copper heater block was then lowered to contact the upper tube holder block. This configuration resulted in poor heat transfer due to contact resistance, misalignment, and conductive losses. To improve heat transfer, the upper holder

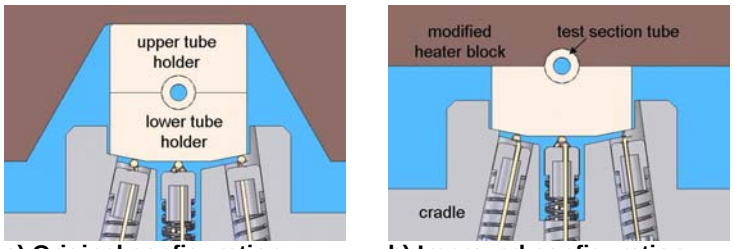

a) Original configuration **b) Improved configuration**

Figure 1. The original configuration resulted in poor heat transfer. Removing the upper tube holder block and modifying the heater block improved performance. The results presented in this paper were obtained from testing of configuration b).

block was removed and a semi-cylindrical groove was machined in the heater block itself, as shown in part b) of Figure 1. This modification resulted in improved alignment and increased heat transfer.

The test section assembly rested in a ceramic instrumentation cradle fabricated from Marinite A, which was selected for its low thermal conductivity. This minimized heat loss through the cradle and support assembly. Spring-loaded thermocouples inserted in the instrumentation cradle measured the temperature of the bottom face of the tube holder block. In addition to the cradle thermocouple measurements, operating conditions were measured at several other locations in the system by thermocouples, pressure transducers, and a Coriolis flow meter.

COMPUTATIONAL CONFIGURATION

The 3-D computational model was constructed based on the system described in the experimental configuration. As shown in Figure 2, the model consists of the cartridge heaters (blue), heater block (green), propellant fluid channel and ancillaries, and a cradle seat (red) to hold the whole assembly. 10.5 million computational cells were placed in the model, with most cells located near the propellant fluid channel walls to capture flow resolution in the boundary layer. Unstructured grids, tetrahedrals, triangular prisms, and pyramids were used for the cells. The computational model considers incompressible flow calculations, i.e. the momentum and energy equations are solved separately. However, RP-2 density changes as a function of temperature are accounted for. The 2-equation realizable k-ε model was chosen for turbulence and a pre-conditioned pressure solver was used in calculations. Spatial discretization is of second-order, with a Total Variation Diminish (TVD) limiter. Temporal discretization employs an implicit scheme, and the Riemann solver is used for diffusion control. Initial computational evaluation indicated that a convergent solution could be obtained with seventy-two hours computational time on thirty-two AMD processors, which perform sixty-four (64) bit operation. The calculations employed an advanced two-layer wall function blended between equilibrium and non-equilibrium functions. Before employing in the 3-D conjugate heat transfer model, validation of the wall treatment in simple pipe flows was performed for two grids: one with y+ less than unity, and the other with y+ greater than 25. The y+ parameter is Reynolds number based on the friction velocity and a grid distance to the wall. When y+ < 5, the grid is inside the viscous sub-layer, and when y+ < 1, the Navier-Stokes equations are solved directly without using wall functions. The purpose of this numerical experiment was twofold: first, to validate the wall function treatment; and second, to save time and effort by examining grid independency of the computation in the simplified model.

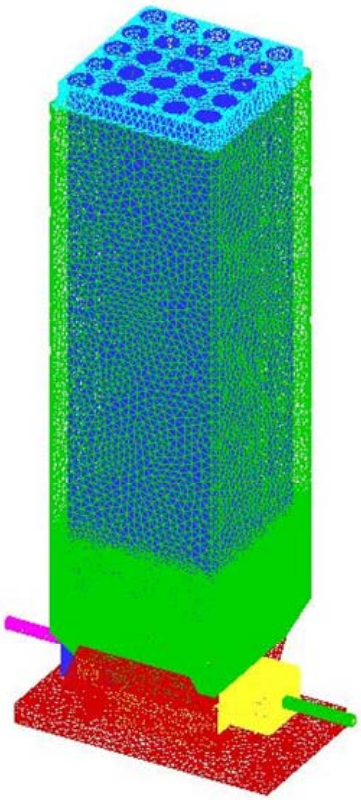

Figure 2. 3-D conjugate heat transfer computational model

RESULTS AND DISCUSSION

EXPERIMENTAL HEAT TRANSFER ANALYSIS

Heat transfer calculations were based on measurements made during only the steady-state heat transfer portion of the experiments. For each data set, this portion was user-defined by examination of outer wall temperature history. The process was considered steady when the

outer wall temperature remained constant within about 5%. For most tests it was constant within 2-3%. Steady-state heat transfer was achieved for between 30-200 s for the data presented here. Outer wall temperatures were then averaged to obtain a representative outer wall temperature for the tube. For most tests, outer wall temperatures varied little along the direction of flow in the tube, justifying the simplification of constant wall temperature. Wetted wall temperature was inferred from outer wall temperature measurements by performing one-dimensional conduction calculations for the top and bottom surfaces, and averaging the resulting inner wall temperatures. This method accounted for the higher temperature on the upper side without neglecting the contribution of heat from the lower surface. The resulting average wetted wall temperature was used to calculate heat transfer results. Data were then time-averaged over the steady-state heat transfer portion of the experiments, so that heat transfer results presented in this paper are based on spatially- and temporally-averaged measurements.

The tube-averaged convective heat transfer coefficient was calculated by:

$$\bar{h} = \frac{\dot{m} c_p}{A_w} ln \frac{T_w - T_{m,i}}{T_w - T_{m,o}} \tag{1}$$

In Eq. (1), $\dot{m}$ is fuel mass flow rate, c_p is specific heat, and A is area. The subscripts i, o, w, and m denote tube inlet, tube outlet, wetted wall, and mean fluid conditions, respectively. Wetted wall temperature was obtained as described above. Mean fluid conditions were treated as those measured in the tube at a downstream location after sufficient mixing occurred. The tube-averaged heat flux was calculated by:

$$\bar{q}'' = \bar{h} \Delta T_{lm} \tag{2}$$

ΔT_{lm}, log mean temperature difference, is determined by:

$$\Delta T_{lm} = \frac{\Delta T_o - \Delta T_i}{ln \frac{\Delta T_o}{\Delta T_i}} \tag{3}$$

Where

$$\Delta T = T_w - T_m \tag{4}$$

The average Nusselt number was obtained with knowledge of the convective heat transfer coefficient, thermal conductivity k and tube inner diameter D:

$$\overline{Nu} \equiv \frac{\bar{h} D}{k} \tag{5}$$

Unless otherwise noted, fluid properties were evaluated at the average bulk fuel temperature, T_b:

$$T_b = \left(T_{m,i} + T_{m,o}\right) / 2 \tag{6}$$

Although physical property data for RP-2 exists, it is currently limited to lower temperatures. However, the comparison between RP-2 and RP-1 properties at these low temperatures is in close agreement. Therefore, RP-1 properties at elevated temperatures were accepted as representative of RP-2. Efforts are currently underway within AFRL to develop a property database anchored by physical measurements in collaboration with NIST.

EXPERIMENTAL RESULTS AND DISCUSSION

Experiments were conducted by prescribing a flow rate and thus fixing the test section velocity and Reynolds Number (Re) at nearly constant values. Within each of these velocity groups, the heater output was gradually increased to achieve a range of test section wall temperatures for a given velocity. Experimental conditions and results are summarized for reference in Table 1. Maximum, minimum, and group-averaged values are given where appropriate. Backpressure, P_o, was measured at the tube outlet. ΔT_m is the mean temperature increase across the test section. T_b, defined in Eq. (6), ranged from 106-160°F.

Table 1. Summary of Experimental Conditions for Heat Flux Testing of RP-2

# of Runs	P_o [psi]	Re (avg.)	V_{ts} (avg.) [ft/s]	Nu (tube-averaged)			T_w (tube-averaged) [°F]			ΔT_m [°F]		
				min	max	avg.	min	max	avg.	min	max	avg.
11	80	5475	26	117	177	150	861	1131	971	80	145	109
7	175	9018	43	207	299	256	841	1009	922	79	132	106
4	530	11031	53	191	227	215	1010	1076	1049	75	91	85
5	230	11332	54	256	360	303	908	1004	958	85	127	104
6	480	16960	81	310	358	336	933	1005	960	70	84	77
5	1720	33179	165	304	362	330	884	1080	977	36	47	41

After the heat transfer results were compiled, experimental data were compared with standard correlations for fully-developed turbulent pipe flow. The correlations, based on empirical data, provide a convenient expression for heat transfer in terms of other non-dimensional parameters, namely Re and Prandtl Number (Pr). More complex correlations have been developed to include the influence of factors such as entrance length effect, friction, and sharp

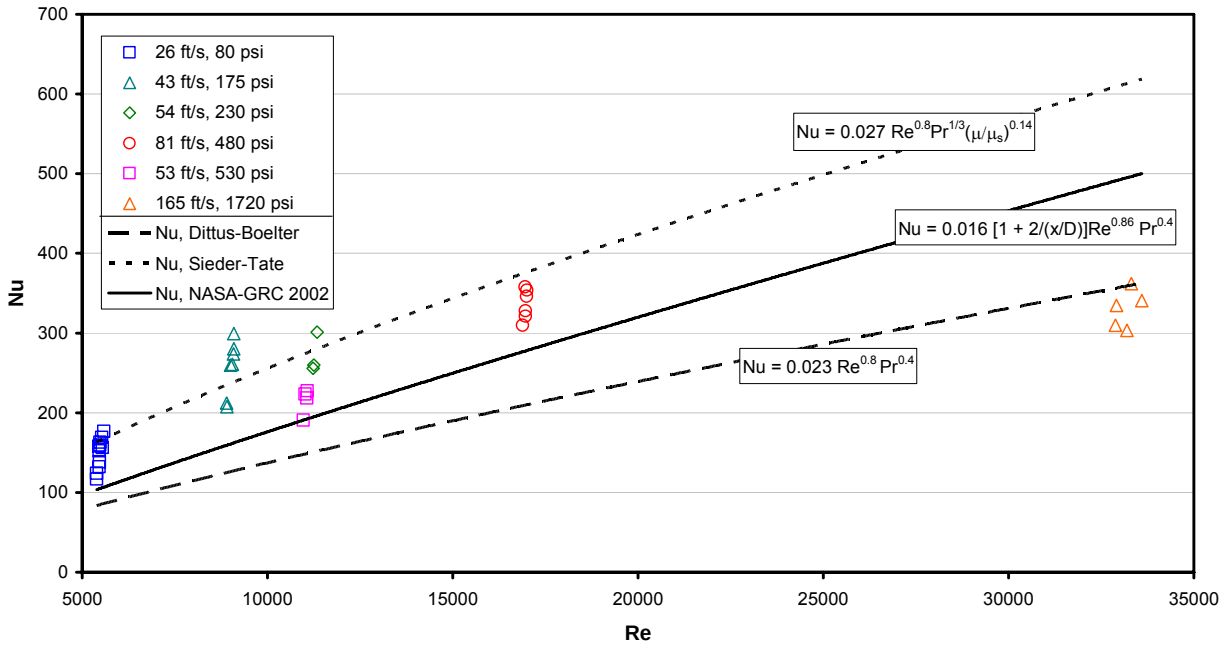

Figure 3. Comparison of experimental data with existing heat transfer correlations: Data are grouped by velocity, with test section backpressure indicated.

fluid property gradients within the flow. Figure 3 compares the measured data with some existing correlations. A first observation is that the Dittus-Boelter equation does not correlate well with the experimental results, even at low Re. This is not surprising, given that although Re and Pr are in the appropriate range (Pr ≈ 27 for all results presented), the Dittus-Boelter correlation does not account for large property variations between the wetted surface and the core flow. Expectedly, the Sieder-Tate correlation, which accounts for large viscosity variations, provides a better representation at lower Re. However, as Re increases, the experimental results follow a different trend than the expected nearly linear relationship to Re. The NASA Glenn Research Center correlation was developed from testing of five aviation hydrocarbon fuels at 1000 psi test section pressure. Again, although a similar Re dependence is seen at low Re, the experimental data is not well correlated at elevated Re. Factors responsible for the discrepancies between the experimental data and the empirical predictions at the upper range of Re number are under further investigation; however, the following are considered to contribute to the observed behaviors.

First, the backpressure was not held constant between tests. Increasing the flow rate was achieved by pressurizing the fuel, so that a higher flow rate was accompanied by higher test section inlet pressure and backpressure. Although the system has the capability of setting backpressure with a flow control valve located downstream of the test section, the valve was typically set at 75% open, allowing a wide range of backpressures. For the lower range of Re in this study, the backpressures were sufficiently low to allow for boiling near the wall which leads to enhancement of heat transfer. At intermediate Re, the backpressures were above critical, but remain sufficiently near to critical to allow for pseudo-boiling transcritical effects to play a role in heat transfer. And at the highest Re, the backpressures were approximately 5 times critical pressure.

Second, large gradients in fuel temperature between the wall and the core flow were present. This was due in part to the short heated test section length (2 in.), which resulted in modest increases in fuel temperature, and therefore low values of bulk fuel temperature, defined in Eq. (6). For high test section wall temperatures, temperature ratios T_w/T_b on the order of 8-10 were common. For hydrocarbons such as RP-2, temperature changes of this magnitude cause significant variation in fuel properties such as density (ρ), thermal conductivity (k), specific heat (c_p), and absolute viscosity (μ), which are used in calculating Re, Pr, and Nu. Therefore, evaluating these properties at the bulk fuel temperature was not justified. Additionally, the temperatures near the wall ranged from the saturation temperature at the test section pressures to above the critical temperature. Therefore, two-phase and supercritical phenomena were expected.

For these reasons, a new correlation accounting for significant variations which affected heat transfer was developed. A correlation of the following form, allowing independent contribution from the various influencing factors, was followed:

$$Nu = K\,Re^{a}\,Pr^{b}\left(\rho/\rho_{w}\right)^{c}\left(\mu/\mu_{w}\right)^{d}\left(k/k_{w}\right)^{e}\left(c_{p}/c_{p,w}\right)^{f}\left(P/P_{crit}\right)^{g} \tag{7}$$

In some cases, the effect of the temperature-dependent properties may be grouped together in a temperature term:

$$Nu = K\,Re^{a}\,Pr^{b}\left(T_{b}/T_{w}\right)^{h}\left(P/P_{crit}\right)^{g} \tag{8}$$

For the current analysis, it was decided to include the separate effect of viscosity gradients, since the ratio of viscosities, (u/u_w) in Eq. (7), was greater than the other property ratios:

$$Nu = K\,Re^{a}\,Pr^{b}\left(T_{b}/T_{w}\right)^{h}\left(P/P_{crit}\right)^{g}\left(\mu/\mu_{w}\right)^{d} \tag{9}$$

At this point, a series of multiple linear regression analyses was performed to obtain a correlation in the form of Eq. (9). From observation of the present data and examination of existing correlations, the coefficients *a* and *b* were held constant at 0.99 and 0.4, respectively. Observation of the data also shows an inverse dependence on the pressure ratio term, i.e. the coefficient *g* must be negative. (For example, see Figure 3 and Table 1 heat transfer results for average Re tests of 11031 and 11332. For similar average wall temperatures, an increase in backpressure causes a decrease in heat transfer.) This is expected physically as the enhancement of heat transfer due to boiling is suppressed at increased pressures. The expected value for coefficient *h* is not as easily determined since the temperature term encompasses the combined effects of several physical properties, all of which change at different rates with increasing temperature. Eventually, the following correlation was determined to most accurately model the current experimental data:

$$Nu = 0.0958\, Re^{0.99}\, Pr^{0.4} \left(P_o/P_{crit}\right)^{-0.161} \left(T_b/T_w\right)^{1.55} \left(\mu_b/\mu_w\right)^{0.0516} \qquad (10)$$

For

$$\begin{bmatrix} 5000 \le Re \le 34{,}000 & eval.at\ T_b \\ Pr \cong 27 & eval.at\ T_b \\ 105^o F \le T_b \le 160^o F & \\ 850^o F \le T_w \le 1150^o F & \\ 70\ psi \le P_o \le 1740\ psi & \end{bmatrix}$$

The subscripts *b*, *w*, *o*, and *crit*, denote bulk, wetted wall, tube outlet, and critical conditions, respectively. A plot of the correlated data is shown in Figure 4 with 20% error bars. The results have been scaled to show Re dependence of the data.

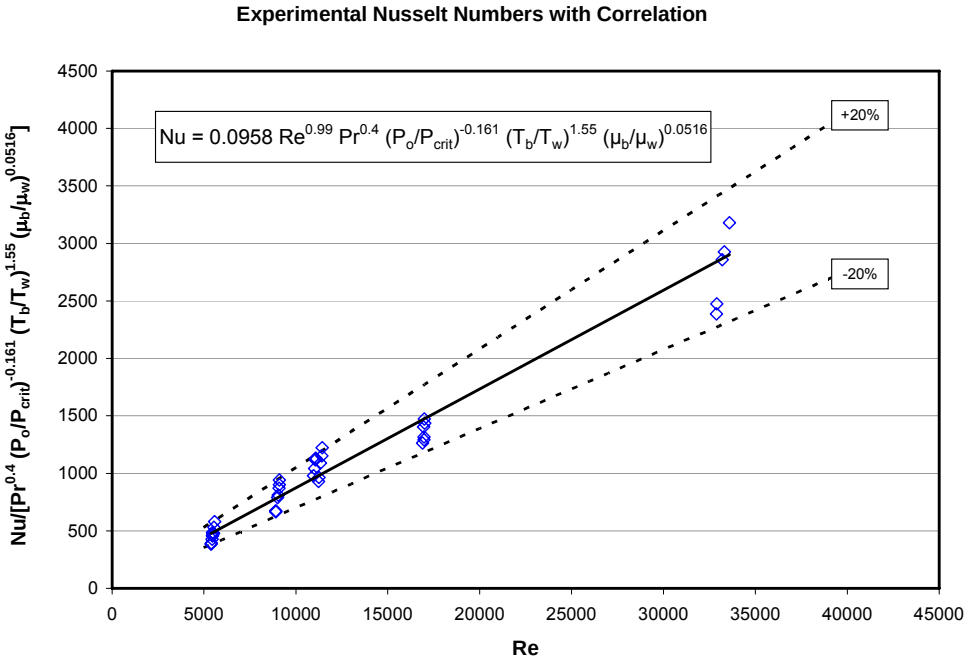

Figure 4. The effects of wall temperature, backpressure, and property variations are accounted for by the developed correlation. The correlation provides a good fit for the experimental data within ±20%.

The effect of backpressure on heat transfer is examined in Figure 5. In part a), heat flux is proportional to wall temperature for a given velocity, as expected from Eq. (2). However, velocity increases it is also expected that tube heat flux should increase at fixed wall temperature, and this was not the observed case for all experiments. At the higher velocities, the effect of pressure on the suppression of boiling and pseudo-boiling is observed. Therefore results were scaled by the pressure ratio term of the correlation in attempt to remove this effect as shown in part b) of the figure. The results show the expected trends in both velocity and wetted wall

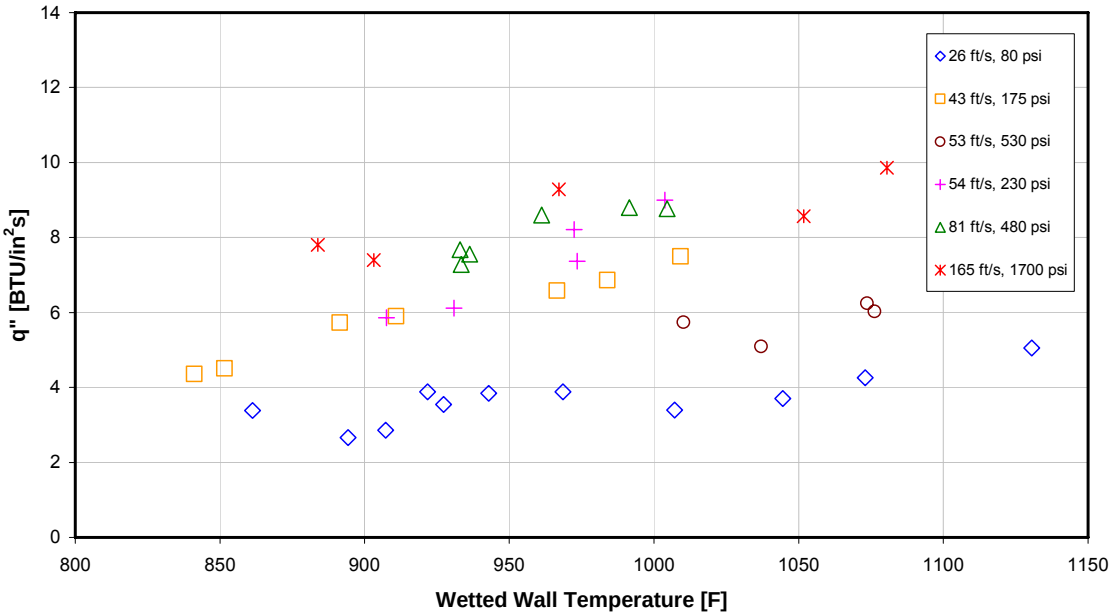

a) Measured heat flux as a function of test section velocity, wall temperature, and backpressure

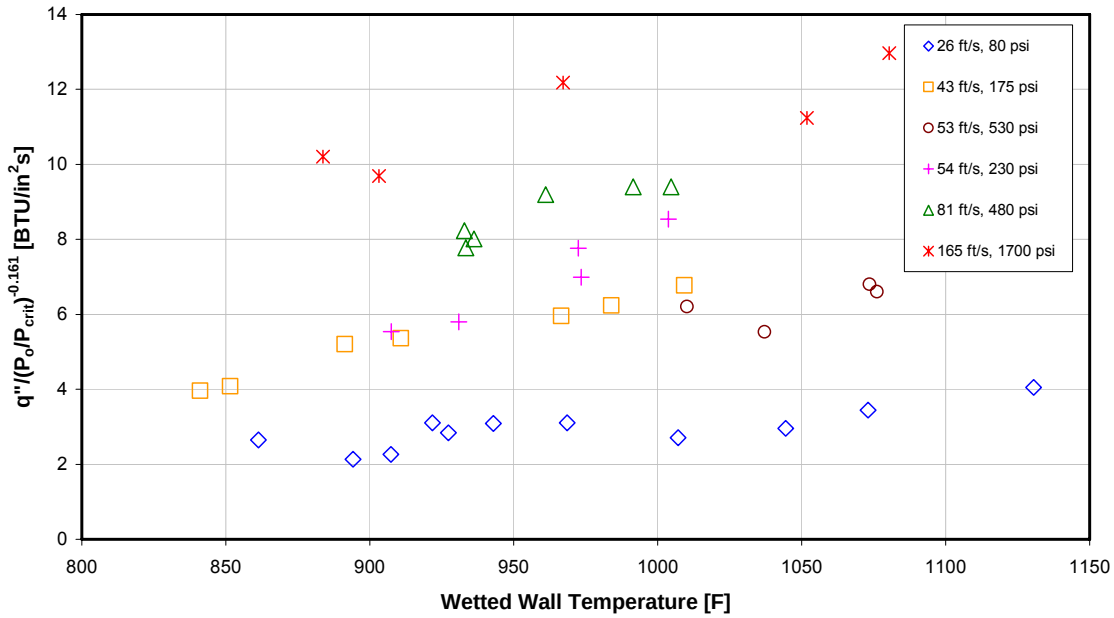

b) Normalized, measured heat flux illustrating the dependence of heat transfer on backpressure

Figure 5. The effects of backpressure on heat transfer are distinguished by normalizing the results by the backpressure term. Pressure-corrected heat fluxes are in general proportional to velocity and wall temperature.

temperature, with some ambiguity when back pressure is near the critical pressure. Further investigation of this complicated effect is planned, especially in the presence of sharp temperature gradients, where physical property variations can be tremendous and effect of very high temperature, low density fluid near the wall can act as an insulting barrier to the cooler outer boundary layer and core flow.

COMPUTATIONAL RESULTS AND DISCUSSION

To validate the advanced two-layer wall functions, four calculations were performed for simple pipe flows in two grids for RP-2. For grids producing y+ < 1, calculations were made with both "solve-to-wall" and advanced two-layer wall function. For grids producing y+ > 25, both "Launder-Spalding" and advanced two-layer wall functions were used. The flow velocity is 75 ft/s, the inlet temperature is 300 K, and the flow is subjected to a wall temperature of 1200 K. The temperature difference between the inlet and outlet of the pipe is documented in Table 2. The results indicate the advanced two-layer wall function produces results comparable to the "solve-to-wall" and "Launder-Spalding" wall functions in the respective cases. The advantage of using the advanced two-layer wall function is that it does not require an extremely fine grid near the wall, which may save substantial computational efforts in 3-D calculations.

Table 2. Comparison of Wall Treatments for Computational Analysis

ΔT [K] for specified wall function			
	Advanced 2-layer	Solve-to-Wall	Launder-Spalding
y+ < 1 grid	67.57	61.19	X
y+ > 25 grid	23.8	X	23.28

The results in Table 2 seem to indicate that grid independency has not been achieved. However, the authors noticed that fluid properties play an important role in heat transfer calculations when employing wall treatments. The dynamic viscosity and thermal conductivity of RP-2 cannot be fit by simple functions provided by CFD++. CFD++ uses an elliptical function to fit the viscosity and a linear curve to fit the thermal conductivity as shown in Figure 6. The discrepancy between solutions obtained by the "solve-to-wall" and "Launder-Spalding" wall function may be a result of the inability to account for correct properties in the calculations.

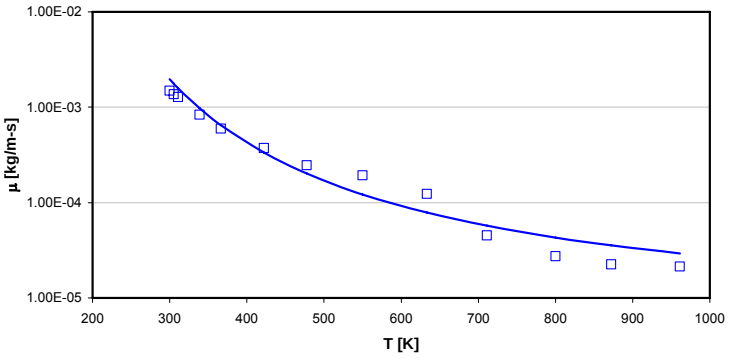

a) Viscosity fit for computations

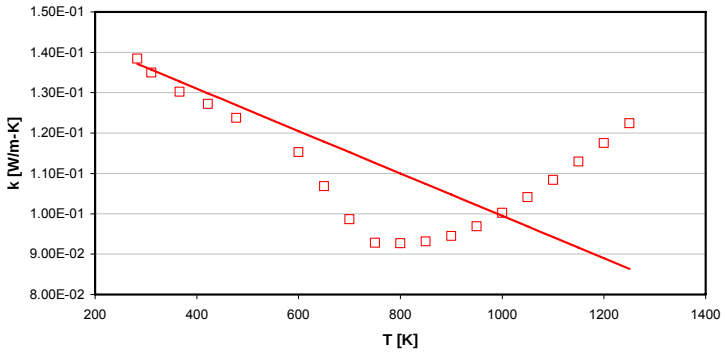

b) Thermal conductivity fit for computations

Figure 6. Computational treatment of physical property variations

Similar calculations using water as the working medium were performed, and the results are presented in Figure 7. When constant properties are assumed for the calculations, the discrepancy between the "solve-to-wall" and "Launder-Spalding" solutions is unbearable, especially at high Reynolds numbers. The agreement when employing correct properties, however, is acceptable. One should note that the flows cover a range of Re from 5,000 to 100,000. The findings here thus establish the importance of the property effects, and it also provides the possibility to establish the grid independency for calculations.

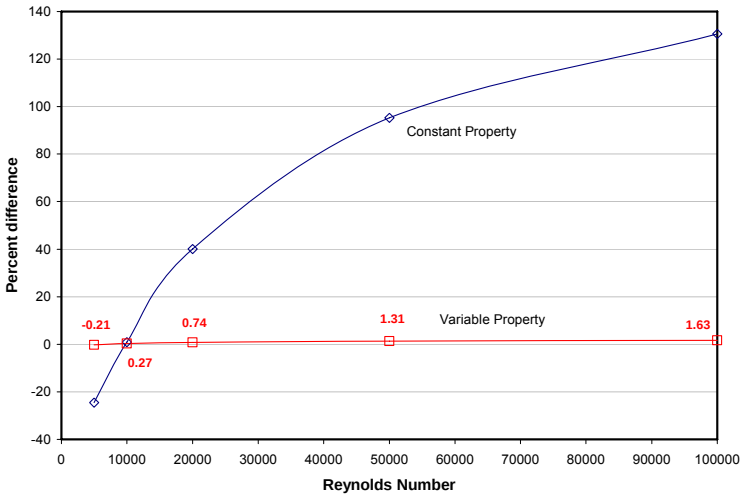

Figure 7. Percentage difference between Launder-Spalding wall function and direct "solve-to-wall" calculation for water

The geometry used for the numerical calculations for the pipe flow under the heat flux condition is as follows: an 8.25-in. long circular tube (0.06-in. ID) is heated circumferentially along a 2-in. section located in the middle of the tube. The average flow speed is 53 fps, and the heated wall has a temperature of 1006 °F. The flow field is shown in Figure 8, and consists of the axial velocity, density, and temperature contour plots. The flow field exhibits a much more complicated behavior than simple pipe flows. The temperature contour shows a thermal boundary layer developed after the heated section, and a corresponding fluid density change is observed in the density contour plot. Downstream of the heated section, the imposed adiabatic wall condition prevents further thickening of the thermal boundary layer However, the density layer continues penetrating into the center core. When RP-2 density decreases at elevated temperature, the flow accelerates to maintain a constant flow rate. This variable density flow is unique in that the flow behavior is pseudo-compressible. The axial velocity contour shows flow accelerating in the center of the pipe in the entrance region as the momentum boundary layer starts to develop. Near the outlet of the pipe, the flow settles to a fully developed flow. However, complicated flow behavior exists in the intermediate region. The particular flow behavior may be a result of velocity disturbances propagating upstream, since pseudo-compressible flow is not of a purely parabolic flow.

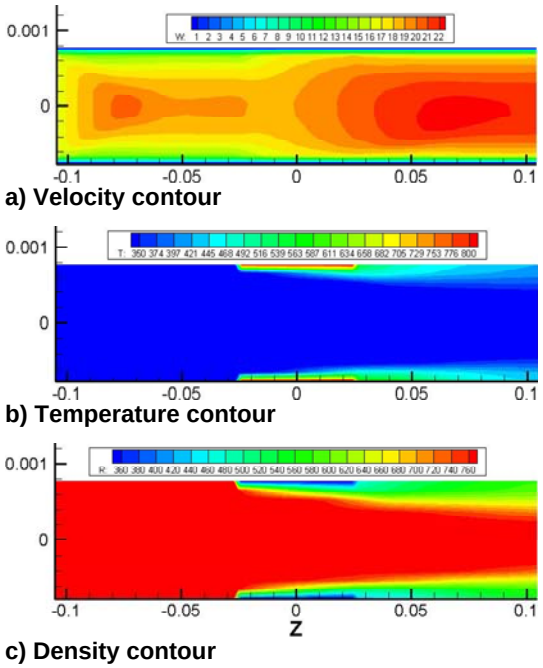

a) Velocity contour

b) Temperature contour

c) Density contour

Figure 8. Flow field contours for 53 ft/s test section velocity, 1006°F wall temperature. Note: The heated section starts at z = -0.0254 and extends to z = 0.0254.

Numerical predictions of Nusselt number were conducted using the wall temperature conditions observed experimentally for three flow velocities: 53 ft/s, 81 ft/s, and 165 ft/s. The results of these computations are presented in Figure 9 and Figure 10. Figure 9 compares numerical and experimental results for 53 ft/s test section velocity. Agreement is poor at 230 psi, where the model does not account for the heat transfer enhancement due to two-phase flow near the wall. However, agreement improves as the back pressure is increased to 530 psi, where the model is physically more realistic.

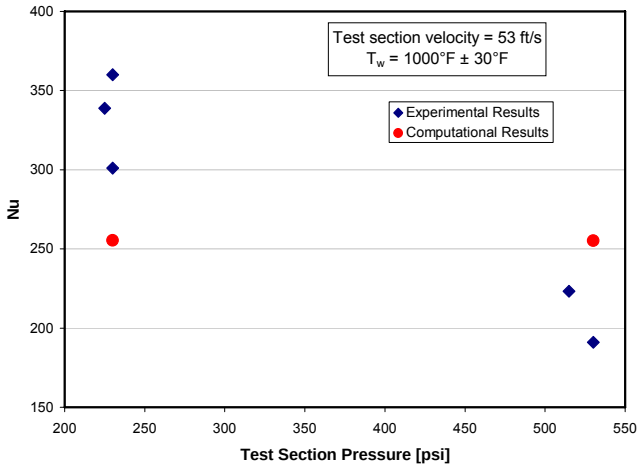

Figure 9. Effects of pressure on heat transfer for constant velocity and wall temperature. As expected, the computation as modeled is insensitive to pressure.

Calculations for the 81 ft/s and 165 ft/s conditions were expected to be in better overall agreement as well, and are shown in Figure 10. In all cases, the numerical predictions are slightly higher than observed in the experiments. The discrepancy at 165 ft/s is not currently understood and further experiments are planned.

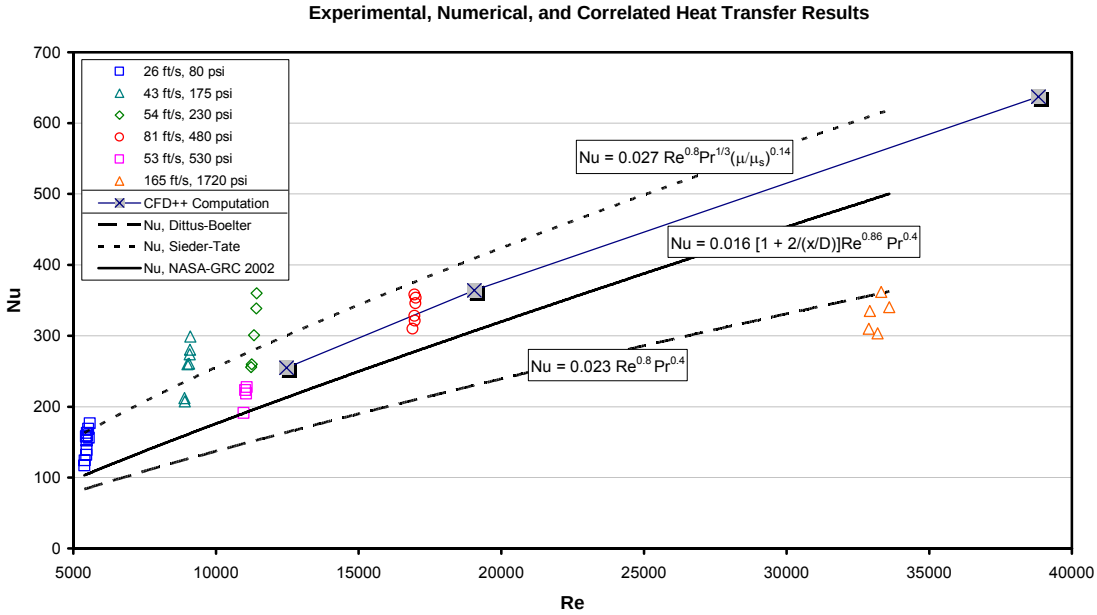

Figure 10. CFD++ computations are in good agreement with experimental data at low Re, but discrepancies at higher Re are observed.

SUMMARY AND CONCLUSIONS

This paper reports recent experiments and numerical simulations of RP-2 cooled thermal stability tests conducted in the AFRL High Heat Flux Facility located at Edwards AFB, CA. Heat transfer measurements and simulations of those experiments using Metacomp's CFD++ conjugate heat transfer capability were conducted over heat fluxes ranging from 2-10 BTU/in^2/s, channel velocities from 26-165 ft/s, and wall temperatures from 840-1135°F. Computational

comparisons with experimental measurements are made and represent the first steps in producing a validated predictive computational capability. A Nusselt number correlation of experimental results for Reynolds numbers between 5,000 and 35,000 was found to capture all data within ±20%. The correlation includes corrections intended to account for complicated effects such as temperature-dependent property variations, sharp thermal gradients near the wall, and pressure effects associated with both boiling at sub-critical pressures and pseudo-boiling above critical pressures.

FUTURE WORK

Future work includes more detailed study of the effect of pressure on heat transfer through experiments. The role of velocity, wall temperature, and heat flux will be examined in both non-coking and coking experiments in order to develop improved models. Coking limits and morphology of deposition, and the roles of sulfur concentration, type, dissolved oxygen concentration, and wetted surface features on thermal decomposition will be evaluated. Validation experiments for the thermal decomposition update to CFD++ will be conducted. Ultimately the authors hope to show experimentally and computationally the detailed physical processes that occur in flows of this nature.

ACKNOWLEDGMENTS

The authors would like to thank Mr. David Hill, Mr. Randy Harvey, Mr. Earl Thomas, Mr. Paul Rue, Ms. Amanda Schoettmer, and Mr. Brett Wight of ERC Inc., Mr. Thomas Werner, Ms. Melinda Martindale, Mr. Jonathan Watts, Dr. Stephen Danczyk, Dr. Ingrid Wysong, of the Air Force Research Laboratory, Edwards AFB, CA, and Mr. Brett Brottlund, Mr. Todd Newkirk, and Mr. Mark Pilgrim of Sverdrup for all their hard work and support throughout the testing in the EC-3 test facility. The authors also would like to thank Mr. Keith Lawson and Mr. Ben Gleason of Edwards AFB, CA for their fabrication support throughout the project.

REFERENCES

1. Bates, R. W., Edwards, J. T., and Meyer, M. L., ***Heat Transfer and Deposition Behavior of Hydrocarbon Rocket Fuels***, Aerospace Sciences Conference AIAA 2003-0123, Reno, NV (Jan 2003)

2. Stiegemeier, B., Meyer, M. L., Taghavi, R., ***A Thermal Stability and Heat Transfer Investigation of Five Hydrocarbon Fuels: JP-7, JP-8, JP-8+100, JP-10, and RP-1***, Joint Propulsion Conference and Exhibit AIAA 2002-3873, Indianapolis, IN (Jul 2002)

3. Giovanetti, A., Spadaccini, L., Szetela, E., ***Deposit Formation and Heat-Transfer Characteristics of Hydrocarbon Rocket Fuels***, Journal of Spacecraft and Rockets, Vol. 22, No. 5, 1985

4. Hines, W. S., ***Heat Transfer to RP-1 Kerosene in Turbulent Flow Under Asymmetric Heating Conditions***, Chemical Engineering Progress Symposium Series, Heat Transfer, pp 193-200

Experimental and Numerical Investigations of RP-2 Under High Heat Fluxes

Matt Billingsley

Simon Lyu

Ron Bates

AFRL/PRSA

Air Force Research Laboratory

Introduction

- Interest in developing reusable, long-life, liquid hydrocarbon fueled rocket engines has continued to grow in recent years
- Air Force Research Laboratory Propulsion Directorate has been developing the capability to examine the thermal performance of newly emerging petroleum distillate fuels such as RP-2, an advanced grade of ultra-low sulfur rocket kerosene
- This work reports initial investigations of heat transfer performance in the AFRL High Heat Flux Facility (HHFF), using RP-2 as a coolant

Experimental Configuration

- **A large copper heater block provided asymmetric heat conductively heated by 25 cartridge heaters**
- **Heaters maintained block temperatures between 900-1400°F measured near the base of the heater block**
- **Spring-loaded T/Cs measured tube holder temperatures**
- **0.125 in. (OD) round copper tubing with 0.032 in. wall thickness was used**

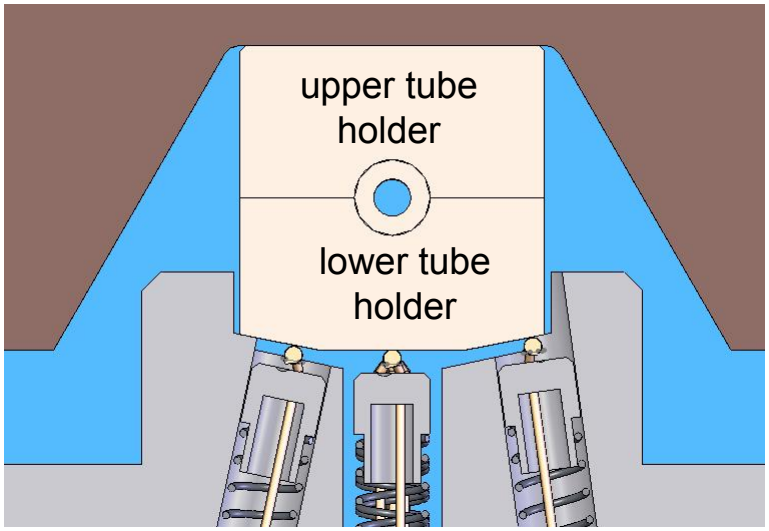

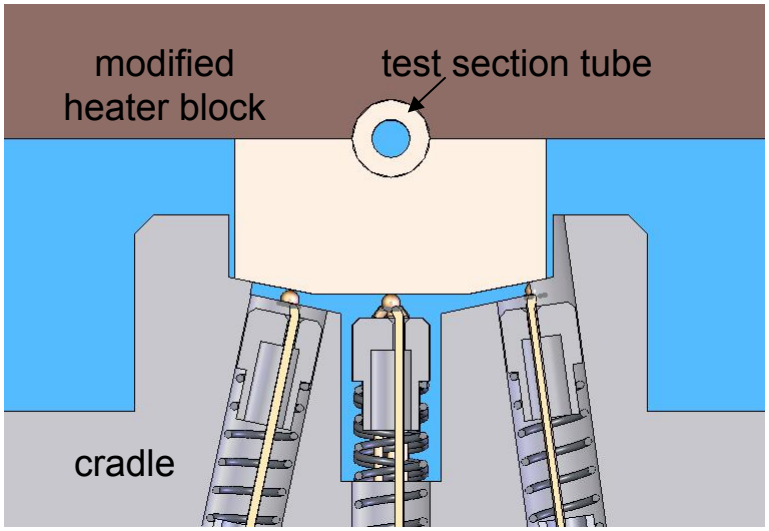

Data Reduction

The tube-averaged convective heat transfer coefficient was calculated by:

$$\bar{h} = \frac{\dot{m} c_p}{A_w} ln \frac{\Delta T_i}{\Delta T_o} \quad (1)$$

Where

$$\Delta T = T_w - T_m \quad (2)$$

The subscripts *i*, *o*, *w*, and *m* denote tube inlet, tube outlet, tube wetted wall, and mean fluid conditions, respectively. Wetted wall temperature was obtained as described above. Mean fluid conditions were treated as those measured in the tube at a downstream location after sufficient mixing occurred. The tube-averaged heat flux was calculated by:

$$\bar{q}'' = \bar{h} \Delta T_{lm} \quad (3)$$

Where ΔT_{lm}, log mean temperature difference, is determined by:

$$\Delta T_{lm} = \frac{\Delta T_o - \Delta T_i}{ln \frac{\Delta T_o}{\Delta T_i}}$$

Data Reduction

The average Nusselt number was obtained with knowledge of the convective heat transfer coefficient, thermal conductivity *k* and tube inner diameter *D*:

$$\overline{Nu} \equiv \frac{\bar{h} D}{k} \tag{5}$$

In many cases, fluid properties were evaluated at the average bulk fuel temperature, T_b:

$$T_b = \left(T_{m,i} + T_{m,o}\right) / 2$$

Summary of Experimental Conditions Measured

Table 1. Summary of Experimental Conditions for Heat Flux Testing of RP-2

# of Runs	P_o psi (kPa)	Re, avg.	V_{ts},avg. ft/s (m/s)	Nu, tube-averaged			T_w, tube-averaged °F (K)			ΔT_m °F (K)		
				min	max	avg.	min	max	avg.	min	max	avg.
11	80 (552)	5475	26 (8)	117	177	150	861 (734)	1131 (884)	971 (795)	80 (44)	145 (81)	109 (61)
7	175 (1207)	9018	43 (13)	207	299	256	841 (723)	1009 (816)	922 (768)	79 (44)	132 (73)	106 (59)
4	530 (3654)	11031	53 (16)	191	227	215	1010 (816)	1076 (853)	1049 (838)	75 (42)	91 (51)	85 (47)
5	230 (1586)	11332	54 (16)	256	360	303	908 (760)	1004 (813)	958 (788)	85 (47)	127 (71)	104 (58)
6	480 (3309)	16960	81 (25)	310	358	336	933 (774)	1005 (814)	960 (789)	70 (39)	84 (47)	77 (43)
5	1720 (11859)	33179	165 (50)	304	362	330	884 (747)	1080 (855)	977 (798)	36 (20)	47 (26)	41 (23)

Correlation

For these reasons, a new correlation accounting for significant variations which affected heat transfer was developed. A correlation of the following form, allowing independent contribution from the various influencing factors, was followed:

$$Nu = K\,Re^{a}\,Pr^{b}\left(\rho/\rho_{w}\right)^{c}\left(\mu/\mu_{w}\right)^{d}\left(k/k_{w}\right)^{e}\left(c_{p}/c_{p,w}\right)^{f}\left(P/P_{crit}\right)^{g} \tag{7}$$

In some cases, the effect of the temperature-dependent properties may be grouped together in a temperature term:

$$Nu = K\,Re^{a}\,Pr^{b}\left(T_{b}/T_{w}\right)^{h}\left(P/P_{crit}\right)^{g} \tag{8}$$

For the current analysis, it was decided to include the separate effect of viscosity gradients, since the ratio of viscosity, (u/uw) in Equation (7), was greater than the other property ratios:

$$Nu = K\,Re^{a}\,Pr^{b}\left(T_{b}/T_{w}\right)^{h}\left(P/P_{crit}\right)^{g}\left(\mu/\mu_{w}\right)^{d} \tag{9}$$

Comparison with Well-known Heat Transfer Correlations

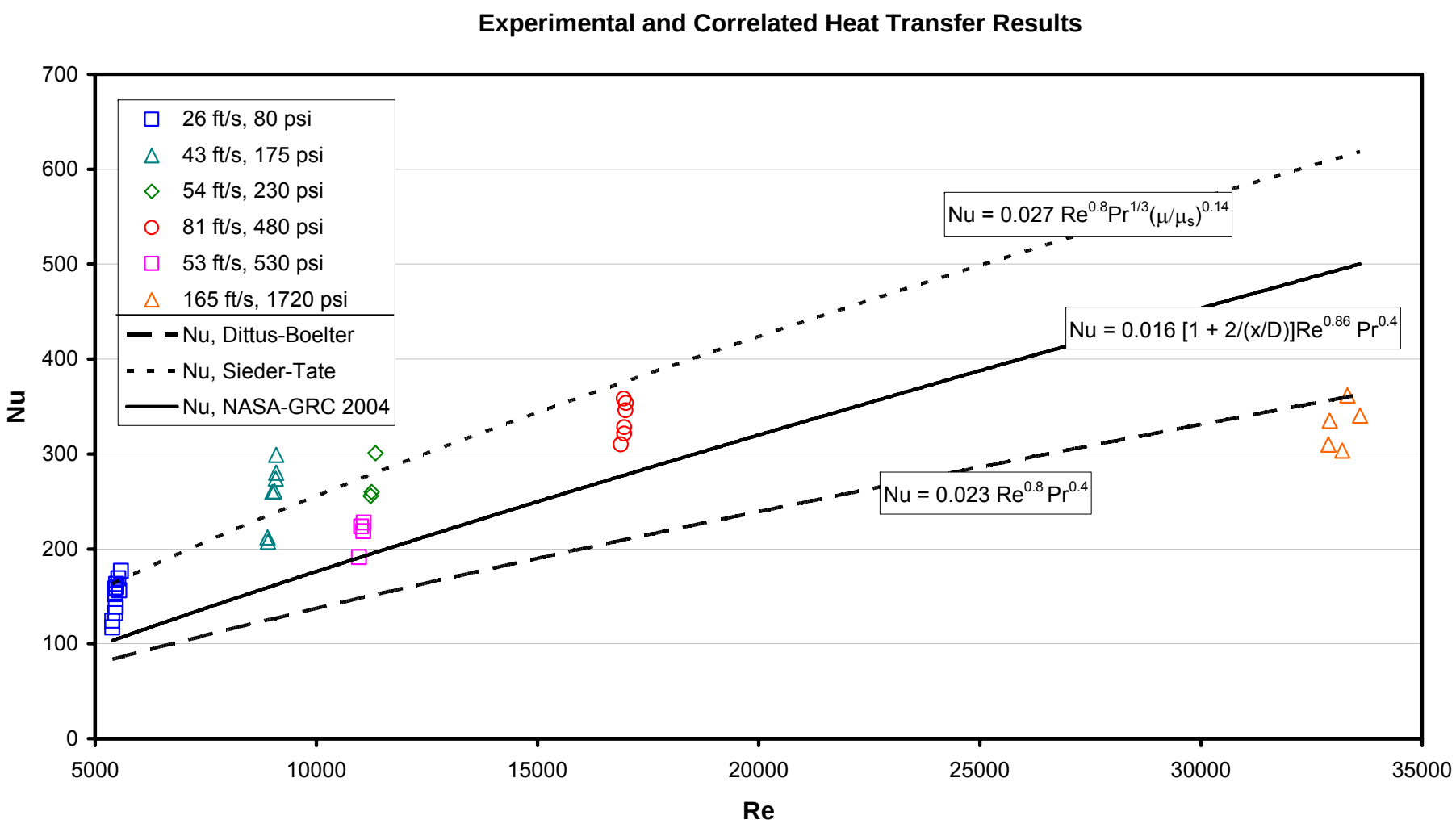

Correlation of Data Result

$$Nu = 0.0958\, Re^{0.99}\, Pr^{0.4} \left(T_b/T_w\right)^{1.55} \left(P_o/P_{crit}\right)^{-0.161} \left(\mu/\mu_w\right)^{0.0516} \qquad (10)$$

For

$$\begin{bmatrix} 5000 \le Re \le 34{,}000 & eval.\,at\ T_b \\ Pr \cong 27 & eval.\,at\ T_b \\ 105^{\circ}F \le T_b \le 160^{\circ}F & \\ 850^{\circ}F \le T_w \le 1150^{\circ}F & \\ 70\,psi \le P_o \le 1740\,psi & \end{bmatrix}$$

- **Correlation accounts for temperature dependant property variations, sharp thermal gradients near the wall, pressure, and well known- Reynolds and Prandtl number effects**

Correlation with Measured Data

Experimental Nusselt Numbers with Correlation

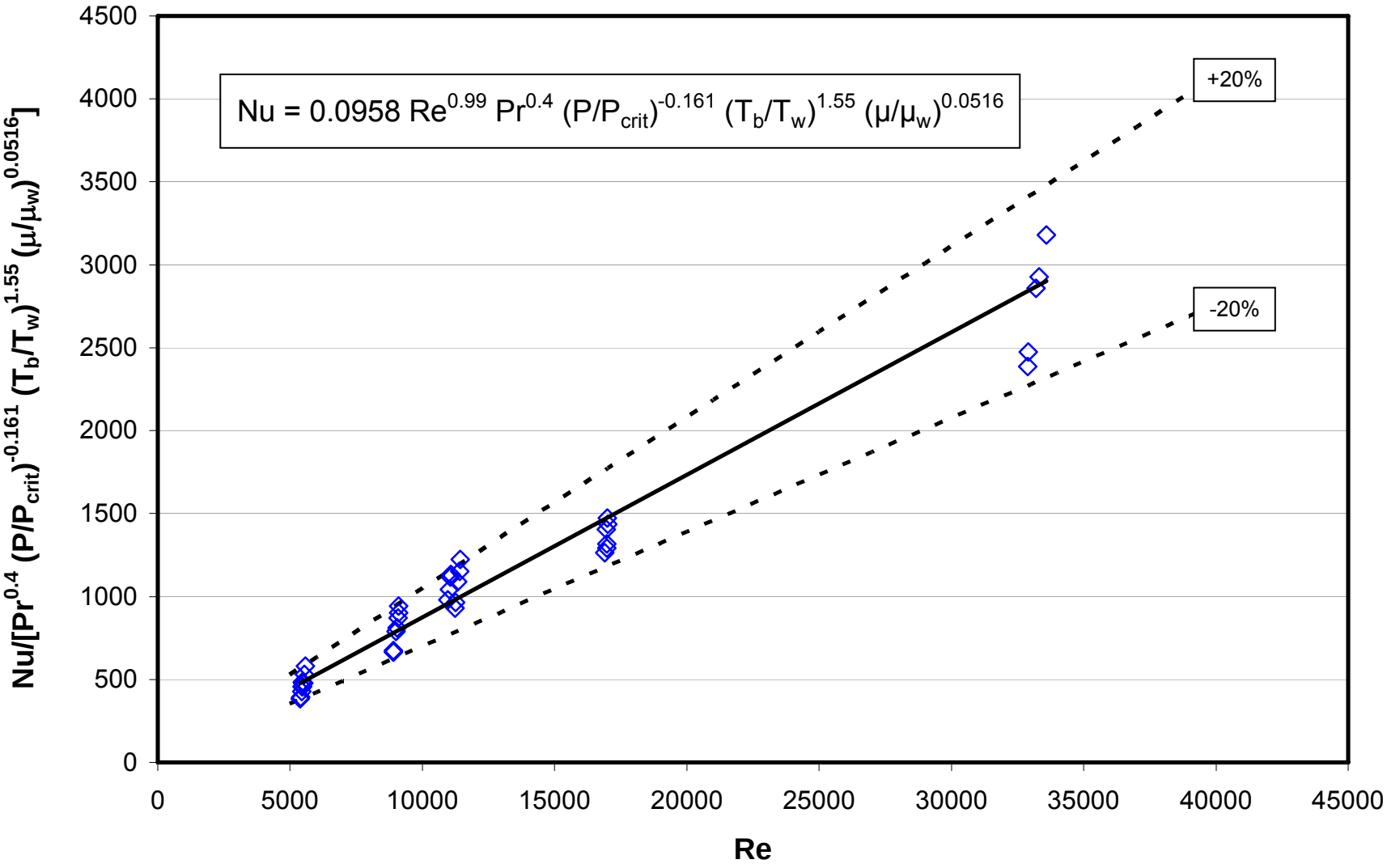

Pressure normalized Tube Heat Flux

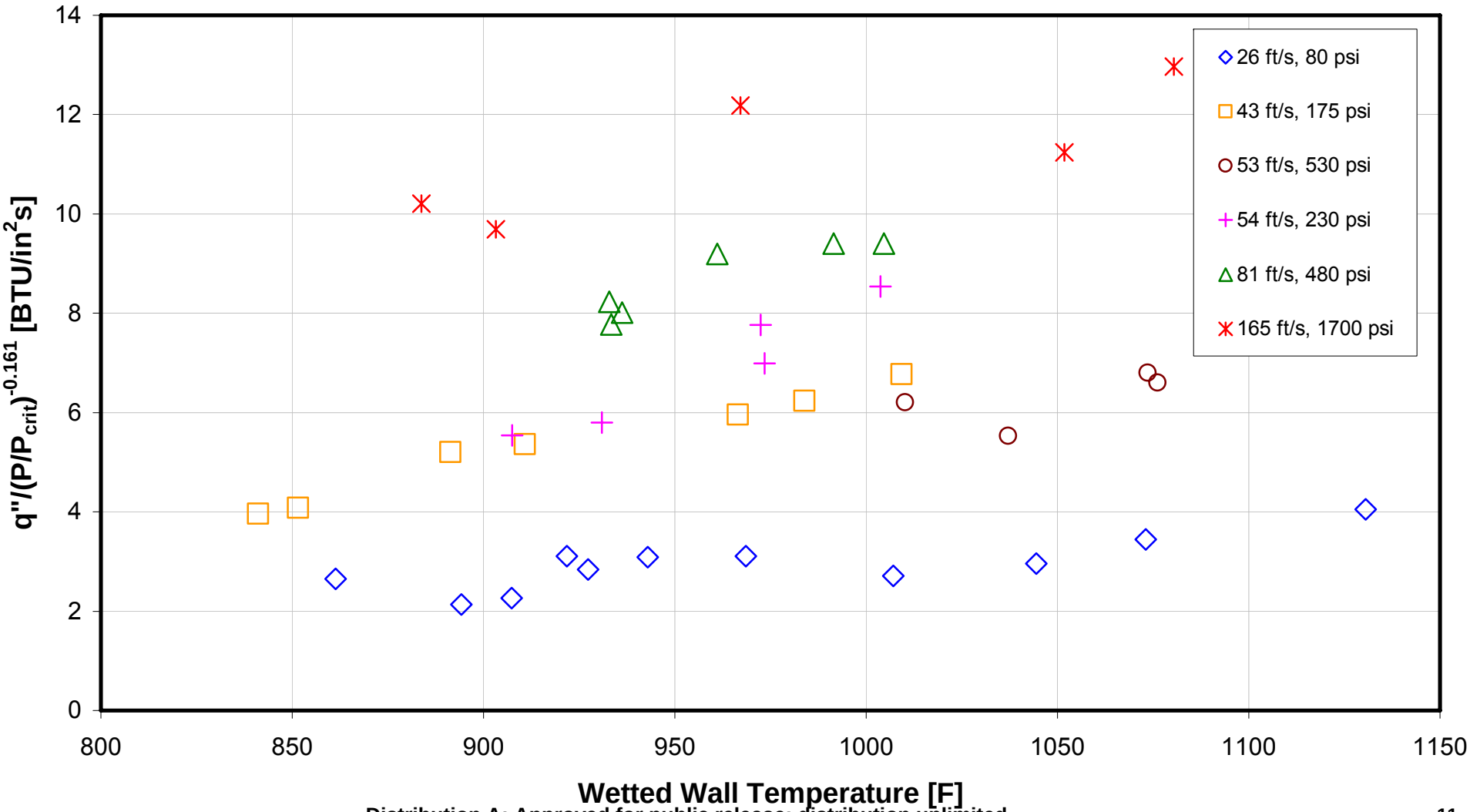

Numerical Model

- 3-D computational model of the cartridge heater (blue), heater block (green), propellant fluid channel and ancillaries, and a cradle seat (red)
- Ten and half million computational cells were placed in the model, with most cells placed in the vicinity of propellant fluid channel walls so that flow resolution around the boundary layer could be captured
- Unstructured grids, tetrahedrals, triangular prisms, and pyramids, made up the cells
- The computational model considers an incompressible flow calculations, however, allowing RP-2 density changes as a function of temperature.
- The turbulence model was chosen to be the 2-equation realizable k-e model
- Spatial discretization is of second-order, with a TVD limiter. Temporal discretization employs an implicit scheme, and the Riemann solver is used for diffusion control.

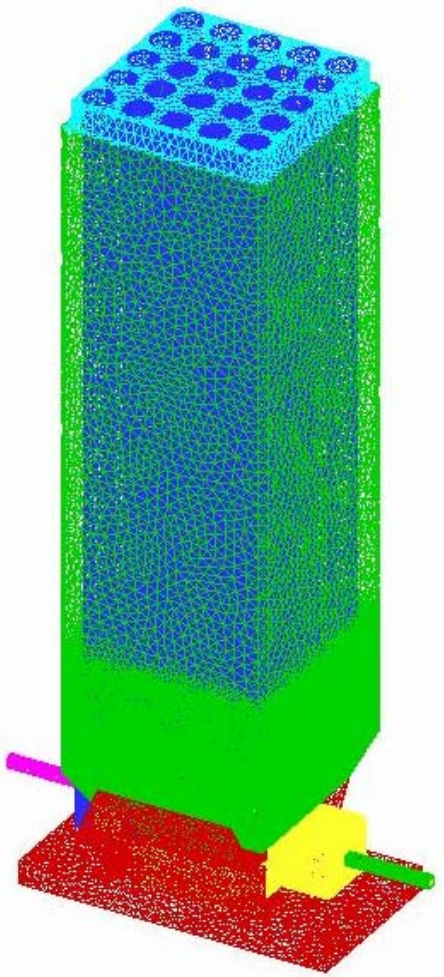

Wall function Check

- To validate the advanced two-layer wall functions, four (4) calculations were performed for simple pipe flows in two grids for RP-2. For grid producing y+ less than unity, calculations were done with both “solve-to-wall” and advanced two-layer wall function. For grid producing y+ greater than 25, both “Launder-Spalding” and advanced two-layer wall functions were used. The flow has a 75 fps speed in the flow channel, the inlet temperature is 300 K, and it is subjected to a 1200-K wall temperature heating.
- The results indicate the advanced two-layer wall function produces comparable results as the “solve-to-wall” and “Launder-Spalding” wall function, in the respective cases, however the effect of variable properties MUST be considered.

Comparison for Water of Wall Function Treatment

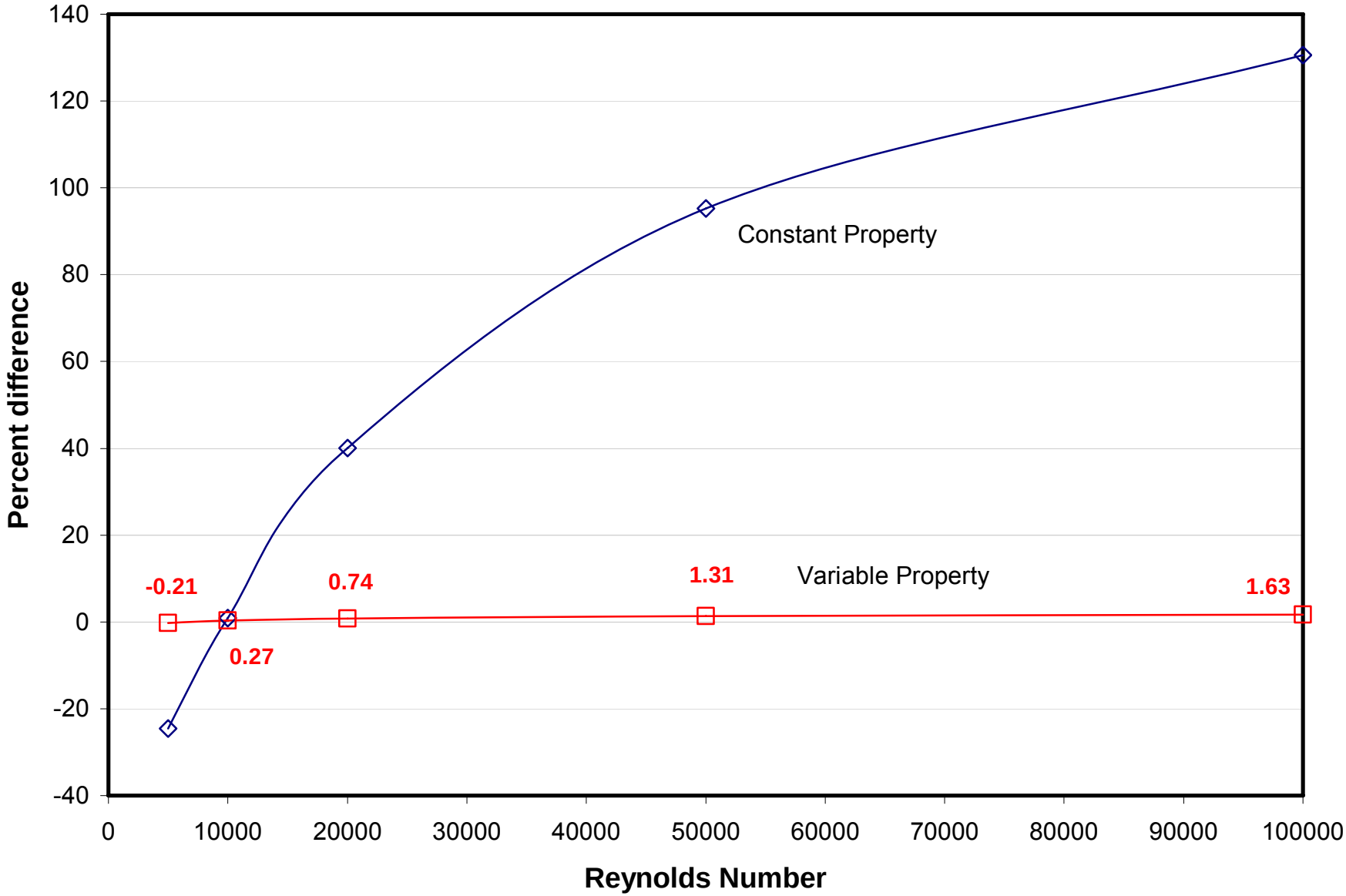

CFD++ Property Fits for Calculations

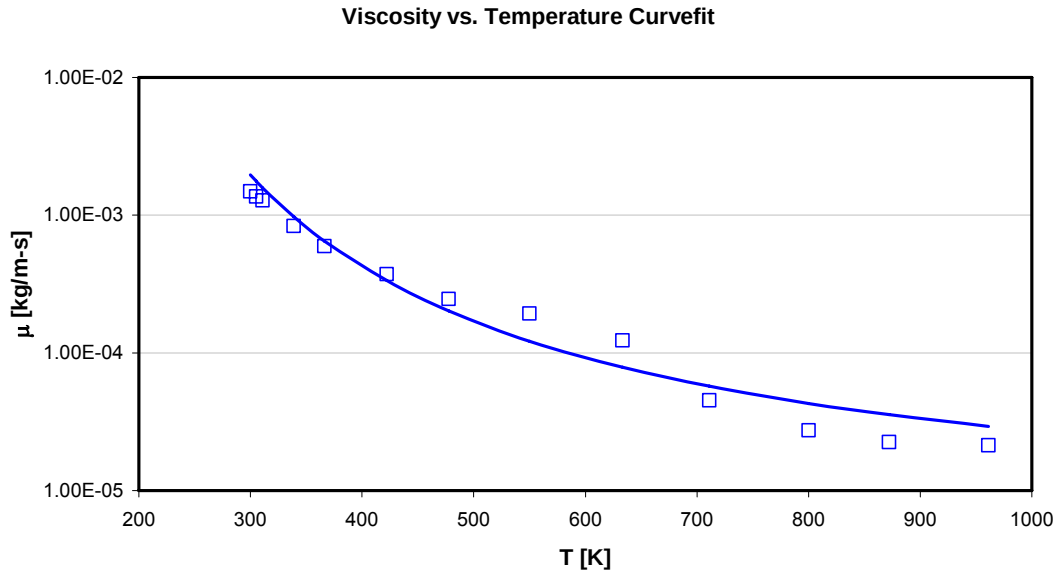

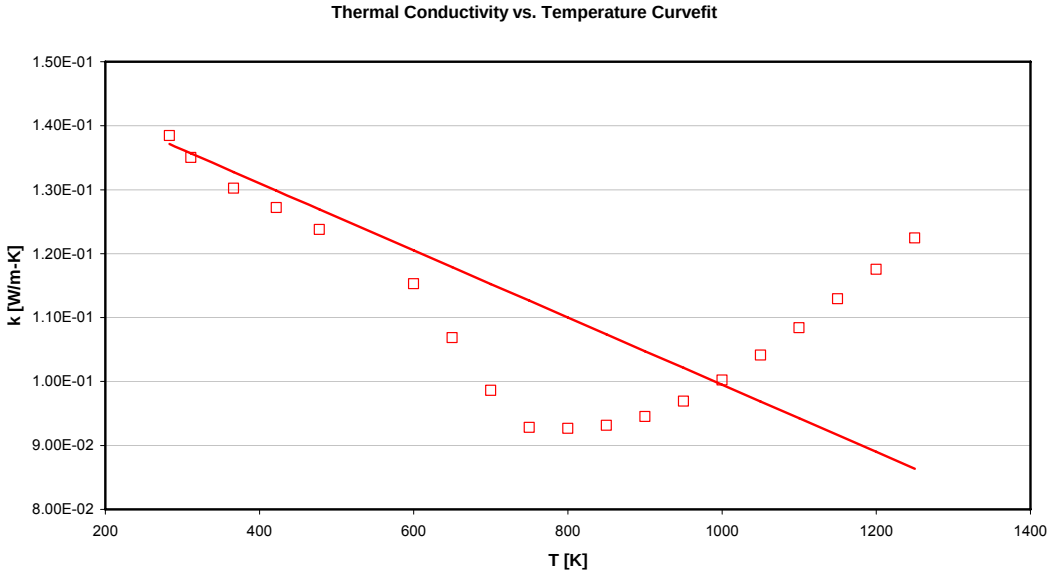

Sample Results from Calculations

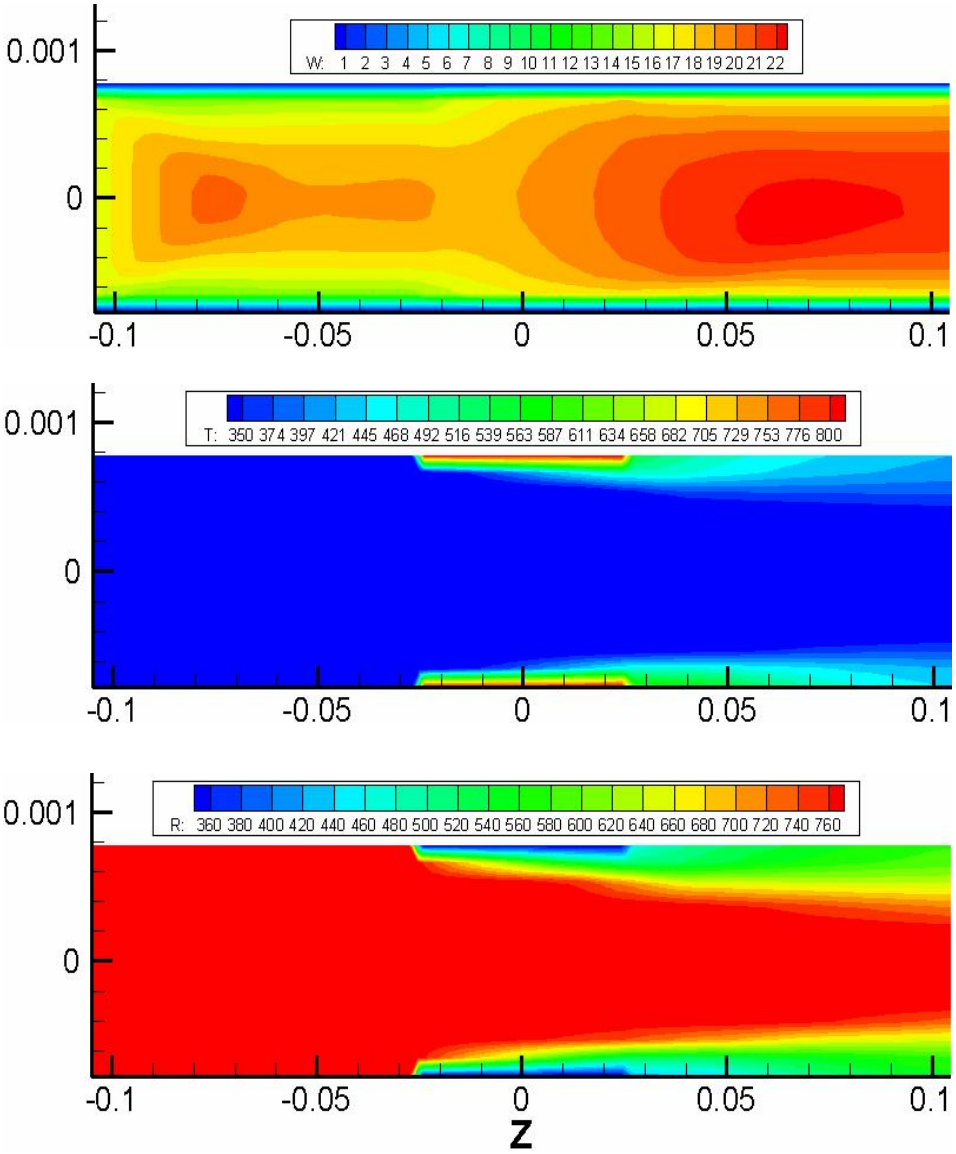

Velocity

Temperature

Density

Comparison of Numerical Prediction at 53 ft/s

Effect of Pressure on Heat Transfer for Constant T_w and Test Section Velocity

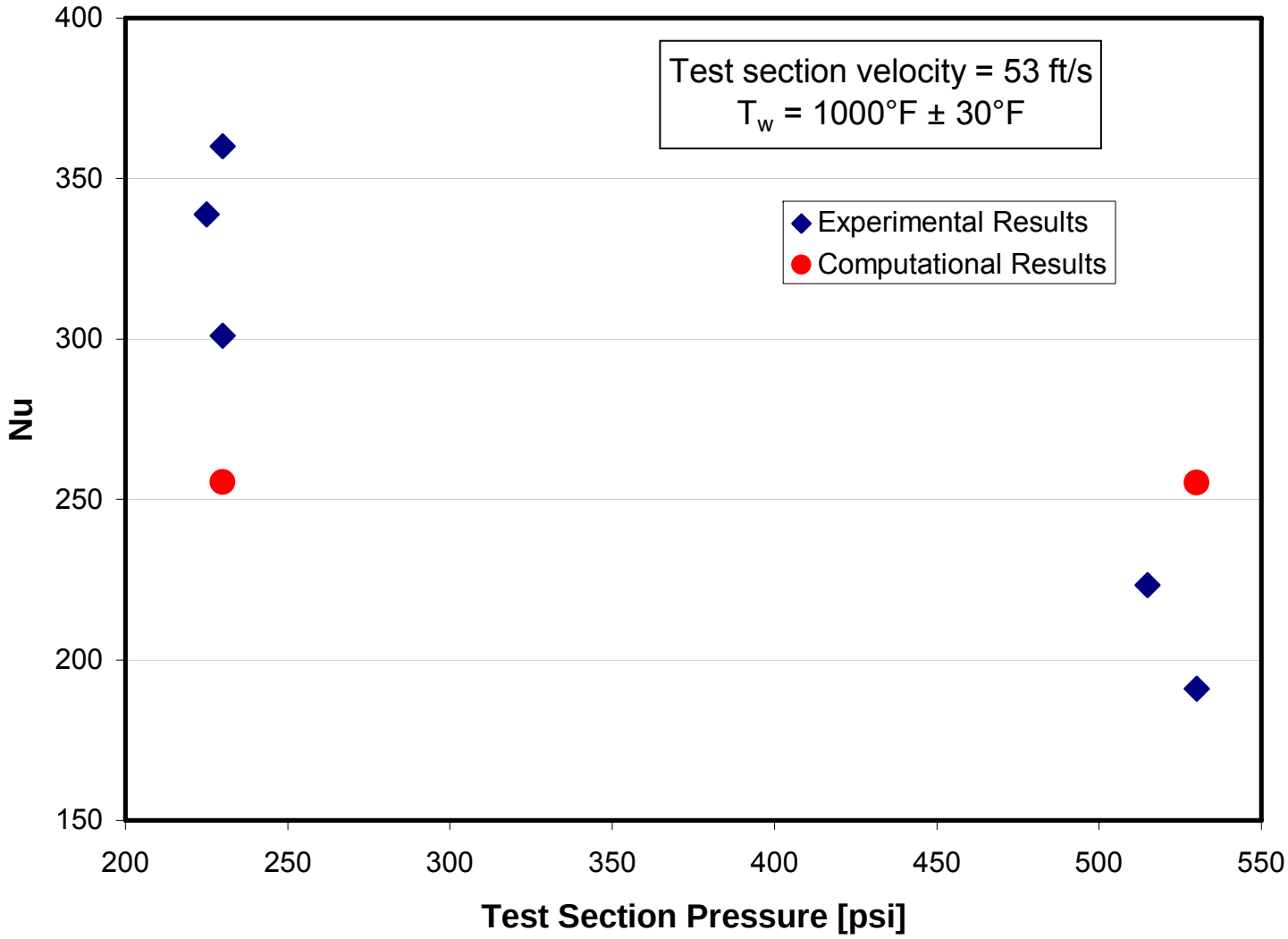

Comparison of Predicted Nu vs Measured Nu

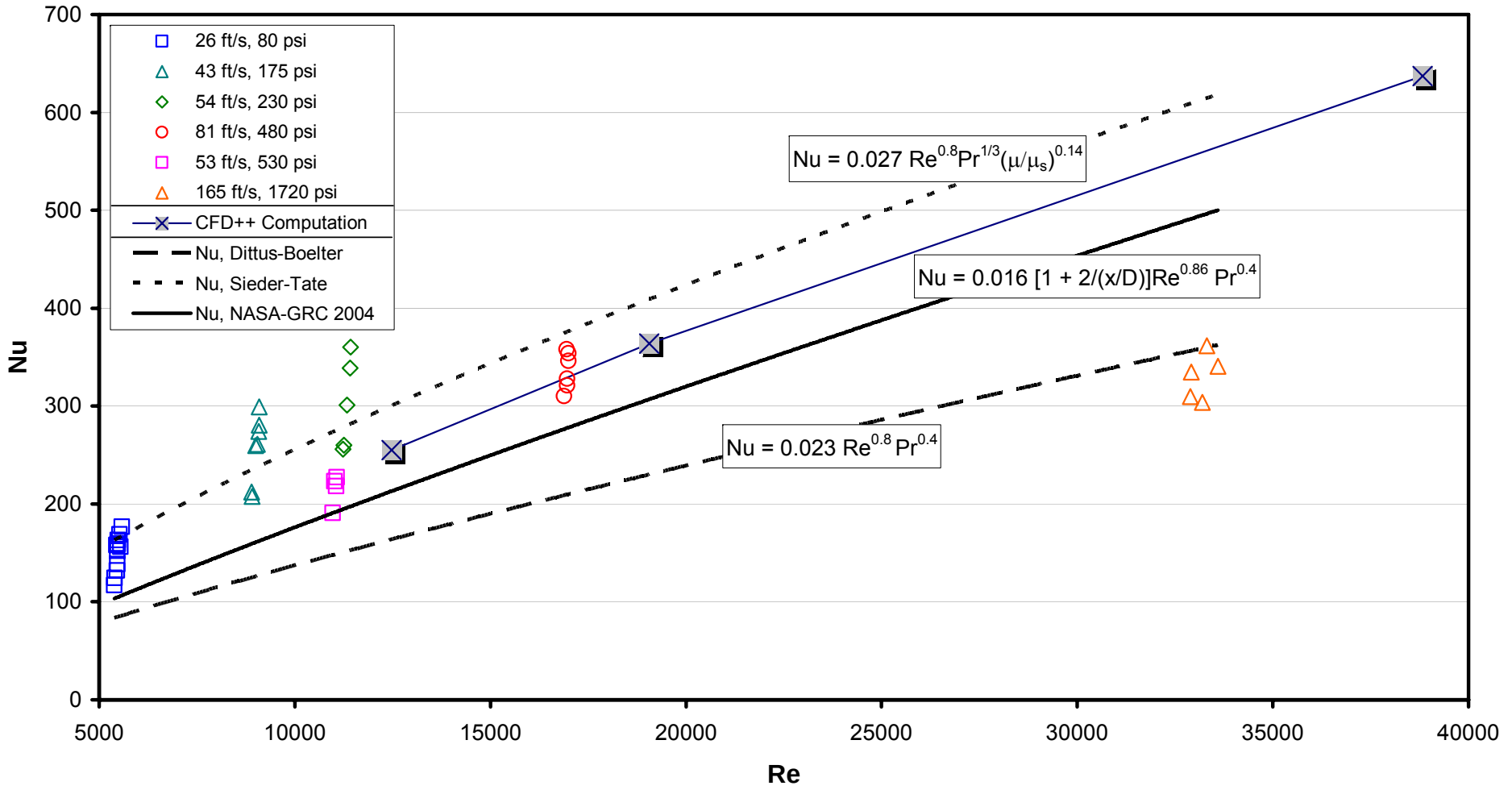

Conclusions

- Experiments and numerical simulations of RP-2 cooled thermal stability tests conducted in the AFRL High Heat Flux Facility located at Edwards AFB, CA over heat fluxes ranging from 2-10 BTU/in2/sec, channel velocities from 26-165 ft/sec, and wall temperatures from 840-1135 F.
- Computational comparisons with experimental measurements were made and represent the first steps in producing a validated predictive computational capability.
- A Nusselt number correlation of experimental results for Reynolds numbers between 5,000-35,000 was found to capture all data within ±20%.
- The correlation includes corrections intended to account for complicated effects such as temperature dependant property variations, sharp thermal gradients near the wall, and pressure effects associated with both boiling at sub-critical pressures and pseudo-boiling above critical pressures.